IOSR Journal of Electrical and Electronics Engineering (IOSR-JEEE)
e-ISSN: 2278-1676,p-ISSN: 2320-3331, Volume 9, Issue 1 Ver. IV (Feb. 2014), PP 20-28
www.iosrjournals.org

Modeling Quantum Effects In The Channel Of A Nanoscale Symmetric Double Gate InAlAs/InGaAs Double Heterostructure HEMT

Neha Verma[1], Enakshi Khular Sharma[2], Jyotika Jogi[1]
[1](*Microelectronics Research Laboratory, Department of Electronic Science, A.R.S.D College, University of Delhi South Campus, New Delhi-110021, India)*
[2](*Department of Electronic Science, University of Delhi South Campus, New Delhi-110021, India)*

Abstract: *This work models the quantization effects dominating a nano-dimensional symmetric InAlAs/InGaAs double heterostructure DG-HEMT (double-gate HEMT). This is done by solving the one-dimensional (1D) time-independent Schrodinger equation in the nanoscale channel comprising of symmetric double triangular quantum well (DTQW) separated by a barrier in the DG-HEMT. The electron confinement due to the finite potential profile of a DTQW is analyzed and eigenenergies and the wave functions are calculated. Effect of the external applied fields at the gates controlling the electron confinement in the channel has been studied. The electron concentration is calculated and its distribution between the two quantum wells in InGaAs channel under the influence of different gate bias has been studied. A shift in electron concentration profile is observed from one well to another by the tunneling phenomenon at different applied electric fields indicating coupling between the two quantum wells. The calculated electron concentration profile obtained at equilibrium has been compared with the simulated results obtained from Quantum moments model and also with a semi-classical model.*
Keywords - *double-gate HEMT, double triangular quantum well (DTQW), eigenenergies, Schrodinger equation, wavefunction.*

I. INTRODUCTION

Quantum heterostructures form the basis of quantum well devices that are now commercially useful products with their superior applications in aeronautics, space, and military communication. Amongst all devices, InP based InAlAs/InGaAs HEMTs are extensively used in microwave circuits and digital IC's and are considered to be the most promising devices for millimeter wave and optical communications due to their superior high frequency and low noise performances [1-2]. The indispensable need of high- speed led to the shrinking of the devices which has been accompanied by short channel effects. The double-gate (DG) technology provided excellent short channel immunity and improved charge control in the channel. Wichmann et al. [3] fabricated a 100 nm InAlAs/InGaAs DG-HEMT using transferred substrate technique with the maximum extrinsic transconductance two times higher than a single-gate HEMT.

As the device size scaling continues to nano-dimensions there is a requirement to model the quantum effects in these devices. In a double heterostructure DG-HEMT, there are two identical heterostructures forming symmetric double quantum wells, where it is assumed that electrons in each well can only have an in-plane motion, as the perpendicular motion is constrained due to quantization. Till now, DG-HEMTs have been analytically modeled with a semi-classical approach for sheet carrier density by treating the two 2-DEGs (two dimensional electron gas) independently with a charge control model neglecting the quantization effects dominating the entire channel [4]. As the de Broglie wavelength of an electron becomes comparable to the thickness of the quantum well the quantization effects cannot be ignored. This requires modeling the two quantum wells formed in double heterostructure DG-HEMT together. The formation of quantum sub-band levels comprising of discrete energy levels and consequently, the wavefunctions corresponding to the values of energy levels describes the quantum state of an electron, which ultimately explains the behavior of nanoscale double quantum wells as a system.

In this paper, quantum modeling of a nano-dimensional channel for a 100 nm double gate InAlAs/InGaAs HEMT is presented. The double quantum wells are treated as a system and the 1D time-independent Schrodinger equation is solved for the potential profile formed in the channel. The potential profile is approximated as double triangular quantum well separated by a barrier in the channel. The eigenenergies and the wavefunctions of an electron confined in the finite potential profile are calculated and studied in the equilibrium condition i.e. when no gate voltage is applied and also under various applied electric fields. From these wavefunctions, the electron concentration under various applied fields is evaluated and this is used to establish an interaction between the two quantum wells.

II. MODEL

The schematic of InAlAs/InGaAs DG-HEMT with gate length 100 nm is shown in Fig. 1. As shown in the figure, there are two identical heterostructures in which both the donor layers are δ-doped and free electrons move from their donor sites to the undoped channel and are confined along the heterointerface on either side of the channel. The electrons from the wide bandgap (InAlAs) layer diffuse to the undoped InGaAs channel layer until equilibrium is reached with the Fermi level (E_F) falling in line. This result in a band bending near the interfaces facilitating the accumulation of electrons in the DTQW formed in the channel.

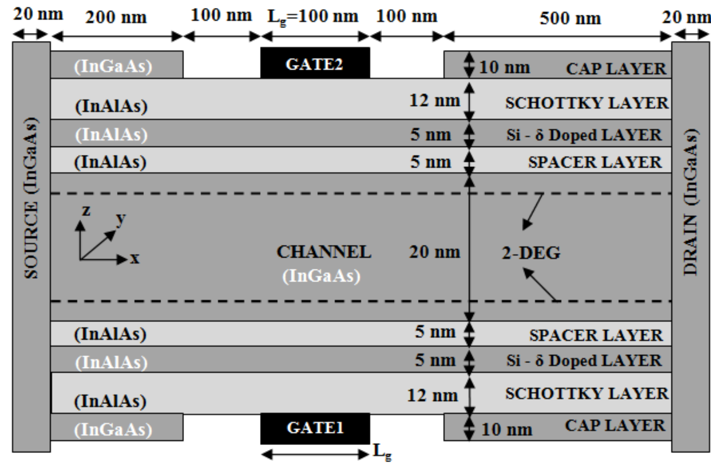

Fig. 1. Structure of InAlAs/InGaAs DG-HEMT.

2.1 Potential Profile in Equilibrium

The energy band-diagram for double heterostructures with two InAlAs/InGaAs junctions at equilibrium results in symmetric double triangular quantum wells separated by a barrier as shown in Fig. 2(a). The potential profile for this DTQW separated by a barrier at equilibrium is obtained using a 3-D ATLAS device simulator (version: 5.16.3.R) [5] and shown as solid lines in Fig. 2(b). The analytical model proposed uses an approximate potential profile *V(z)* as shown by dotted lines in Fig. 2(b) and defined as follows:

$$V(z) = \begin{cases} V_0 \cdot \left(\dfrac{-2a - z}{a} \right), & z \le -2a \\ V_1 \cdot \left(\dfrac{z + 2a}{a} \right), & -2a \le z \le -a \\ V_1, & |z| \le a \\ V_1 \cdot \left(\dfrac{2a - z}{a} \right), & a \le z \le 2a \\ V_0 \cdot \left(\dfrac{z - 2a}{a} \right), & z \ge 2a \end{cases} \tag{1}$$

where, V_0 represents the conduction band discontinuity and V_1 is the height of the barrier between the two quantum wells. The origin is taken at the centre, the barrier thickness and the width of each well are taken as 2a where 'a' is one sixth of the channel width.

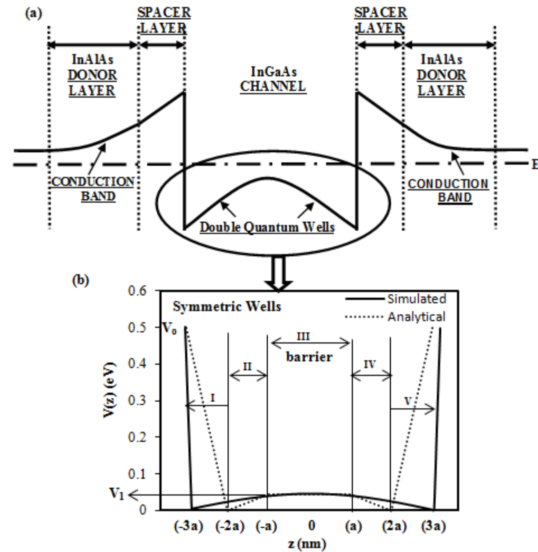

Fig. 2. Channel of DG-HEMT (a) Energy Band diagram for double heterostructures with symmetric double quantum wells. (b) Potential profile of a symmetric DTQW separated by a barrier formed in the channel at equilibrium.

Since the potential profile is symmetric about the z=0 axis, it is sufficient to consider only the region $0 \le z \le 3a$. The one dimensional time-independent Schrodinger equation for the region $0 \le z \le 3a$ can be written as follows:

2.1.1 For one half of the barrier i.e. $0 \le z \le a$ *:*

$$\frac{d^2\psi(z)}{dz^2} - k^2\psi(z) = 0, \tag{2}$$

where ψ is the wavefunction, $k^2 = [2m^*/\hbar^2]\cdot[V(z) - E]$, E is the energy eigenvalue, $\hbar$ is the reduced Planck constant, m^* is the effective mass of the electron.

2.1.2 For the regions $a \le z \le 2a$ *and* $z \ge 2a$ *:*

The Schrodinger equation reduces to the Airy equation:

$$\frac{d^2\psi}{d\xi^2} - \xi\psi = 0 \tag{3}$$

where the new variable ξ is defined as:

$$\xi_{IV} = \left(\frac{V_1 \cdot \pi^2}{\left(\hbar^2\pi^2/2m^*a^2\right)}\right)^{1/3} \cdot \left[\left(\frac{2a - z}{a}\right) - \frac{E}{V_1}\right] \text{ for } a \le z \le 2a, \tag{4}$$

$$\xi_V = \left(\frac{V_0 \cdot \pi^2}{\left(\hbar^2\pi^2/2m^*a^2\right)}\right)^{1/3} \cdot \left[\left(\frac{z - 2a}{a}\right) - \frac{E}{V_0}\right] \text{ for } z \ge 2a \tag{5}$$

The solutions of (3) are the Airy functions with the respective ξ as their argument.

2.1.3 Symmetric Solutions

The wavefunction ψ_s for the symmetric state will have a solution as follows:

$$\psi_s(z) = \begin{cases} C_{s1} \cdot \cosh(kz), & 0 \le z \le a \\ C_{s2} \cdot Ai(\xi_{sIV}) + D_{s2} \cdot Bi(\xi_{sIV}), & a \le z \le 2a \\ C_{s3} \cdot Ai(\xi_{sV}), & z \ge 2a \end{cases} \tag{6}$$

where *Ai* and *Bi* are the regular and the irregular Airy functions and the variables ξ_{sIV} and ξ_{sV} correspond to the symmetric case. The boundary conditions for continuity of ψ_s and $d\psi_s / dz$ at $z=a$ and $z=2a$, lead to the following determinant for the four homogenous equations in C_{s1}, C_{s2}, D_{s2} and C_{s3}:

$$\begin{vmatrix} \cosh(ka) & -Ai(\xi_{sIV}{}^{a}) & -Bi(\xi_{sIV}{}^{a}) & 0 \\ k\sinh(ka) & \chi_1 Ai'(\xi_{sIV}{}^{a}) & \chi_1 Bi'(\xi_{sIV}{}^{a}) & 0 \\ 0 & Ai(\xi_{sIV}{}^{2a}) & Bi(\xi_{sIV}{}^{2a}) & -Ai(\xi_{sV}{}^{2a}) \\ 0 & -\chi_1 Ai'(\xi_{sIV}{}^{2a}) & -\chi_1 Bi'(\xi_{sIV}{}^{2a}) & -\chi_0 Ai'(\xi_{sV}{}^{2a}) \end{vmatrix} \quad (7)$$

where $\xi_{sIV}{}^{a}$ is $\xi_{sIV}\big|_{z=a}$, $\xi_{sIV}{}^{2a}$ is $\xi_{sIV}\big|_{z=2a}$, $\xi_{sV}{}^{2a}$ is $\xi_{sV}\big|_{z=2a}$ and

$$\chi_{1,0} = \left[\left(\frac{V_{1,0} \cdot \pi^2}{\left(\hbar^2 \pi^2 / 2m^* a^2\right)} \right)^{1/3} \cdot \left(\frac{1}{a} \right) \right] \quad (8)$$

For non trivial solutions, the determinant in (7) has to be zero giving the eigenvalue equation which can be solved to obtain the values of *E*.

2.1.4 Antisymmetric Solutions

Similarly wavefunction for antisymmetric state (ψ_{as}) is obtained as:

$$\psi_{as}(z) = \begin{cases} C_{as1} \cdot \sinh(kz), & 0 \le z \le a \\ C_{as2} \cdot Ai(\xi_{asIV}) + D_{as2} \cdot Bi(\xi_{asIV}), & a \le z \le 2a \\ C_{as3} \cdot Ai(\xi_{asV}), & z \ge 2a \end{cases} \quad (9)$$

The boundary conditions for continuity of ψ_{as} and $d\psi_{as}/dz$ at $z=a$ and $z=2a$, lead to the following determinant for the four homogenous equations in C_{as1}, C_{as2}, D_{as2} and C_{as3}:

$$\begin{vmatrix} \sinh(ka) & -Ai(\xi_{asIV}{}^{a}) & -Bi(\xi_{asIV}{}^{a}) & 0 \\ k\cosh(ka) & \chi_1 Ai'(\xi_{asIV}{}^{a}) & \chi_1 Bi'(\xi_{asIV}{}^{a}) & 0 \\ 0 & Ai(\xi_{asIV}{}^{2a}) & Bi(\xi_{asIV}{}^{2a}) & -Ai(\xi_{asV}{}^{2a}) \\ 0 & -\chi_1 Ai'(\xi_{asIV}{}^{2a}) & -\chi_1 Bi'(\xi_{asIV}{}^{2a}) & -\chi_0 Ai'(\xi_{asV}{}^{2a}) \end{vmatrix} \quad (10)$$

where $\xi_{asIV}{}^{a}$ is $\xi_{asIV}\big|_{z=a}$, $\xi_{asIV}{}^{2a}$ is $\xi_{asIV}\big|_{z=2a}$ and $\xi_{asV}{}^{2a}$ is $\xi_{asV}\big|_{z=2a}$.

2.2 Potential Profile under applied Electric Field

The Schrodinger equation for the DTQW system separated by a barrier under an applied electric field as shown in Fig. 3 is given by:

$$\frac{d^2\psi(z)}{dz^2} - \frac{2m^*}{\hbar^2}\left[V_{eff}(z) - E\right] \cdot \psi(z) = 0 \quad (11)$$

where the effective potential $V_{eff}(z)$ is given by:

$$V_{eff}(z) = \begin{cases} V_0 \cdot \left(\frac{-2a - z}{a} \right) + (eFz), & z \le -2a \\ V_1 \cdot \left(\frac{z + 2a}{a} \right) + (eFz), & -2a \le z \le -a \\ V_1 + (eFz), & |z| \le a \\ V_1 \cdot \left(\frac{2a - z}{a} \right) + (eFz), & a \le z \le 2a \\ V_0 \cdot \left(\frac{z - 2a}{a} \right) + (eFz), & z \ge 2a \end{cases} \quad (12)$$

where e is the electron charge.

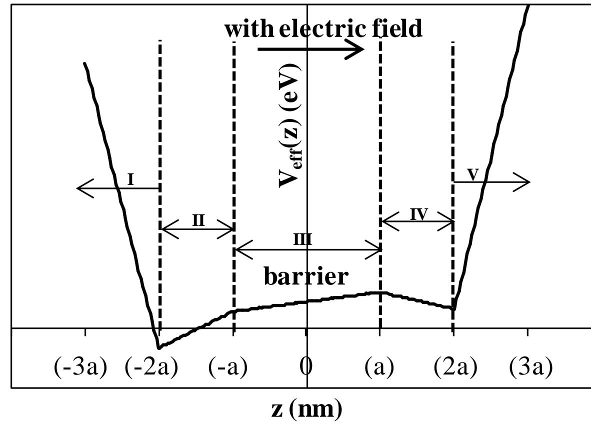

Fig. 3. Potential profile of DTQW separated by a barrier formed in the channel with applied electric field.

Redefining variable ξ in the regions: I $(z \le -2a)$, II $(-2a \le z \le -a)$, III $(-a \le z \le a)$, IV $(a \le z \le 2a)$, and V $(z \ge 2a)$ as:

$$\xi_{I,V} = \alpha_{I,V} \cdot \left[\mp z\left(1 \mp \frac{eFa}{V_0}\right) - a\left(2 + \frac{E}{V_0}\right)\right], \tag{13}$$

$$\xi_{II,IV} = \alpha_{II,IV} \cdot \left[\pm z\left(1 \pm \frac{eFa}{V_1}\right) + a\left(2 - \frac{E}{V_1}\right)\right], \tag{14}$$

$$\xi_{III} = \alpha_{III} \cdot \left[E - V_1 - eFz\right] \tag{15}$$

where

$$\alpha_{I,V} = \left[\frac{\left(2m^* V_0 / a\hbar^2\right)}{\left(1 \mp eFa/V_0\right)^2}\right]^{1/3}, \quad \alpha_{II,IV} = \left[\frac{\left(2m^* V_1 / a\hbar^2\right)}{\left(1 \pm eFa/V_1\right)^2}\right]^{1/3} \text{ and } \quad \alpha_{III} = -\left[2m^* / \left(e\hbar F\right)^2\right]^{1/3} \tag{16}$$

Equation (11) reduces to the Airy equation (3) whose solutions are the Airy functions with the respective ξ as their argument. So, the wavefunction $\psi(z)$ may be written as:

$$\psi(z) = \begin{cases} C_1 \cdot Ai(\xi_I) + D_1 \cdot Bi(\xi_I), & z \le -2a \\ C_2 \cdot Ai(\xi_{II}) + D_2 \cdot Bi(\xi_{II}), & -2a \le z \le -a \\ C_3 \cdot Ai(\xi_{III}) + D_3 \cdot Bi(\xi_{III}), & |z| \le a \\ C_4 \cdot Ai(\xi_{IV}) + D_4 \cdot Bi(\xi_{IV}), & a \le z \le 2a \\ C_5 \cdot Ai(\xi_V) + D_5 \cdot Bi(\xi_V), & z \ge 2a \end{cases} \tag{17}$$

The boundary conditions at $|z| = a, 2a$ leads to eight homogenous equations for the coefficients C_j (j=1-5) and D_k (k=1-5) which can be written as:

$$\begin{bmatrix} C_2 \\ D_2 \end{bmatrix} = [M_1] \cdot \begin{bmatrix} C_1 \\ D_1 \end{bmatrix}, \begin{bmatrix} C_3 \\ D_3 \end{bmatrix} = [M_2] \cdot \begin{bmatrix} C_2 \\ D_2 \end{bmatrix}, \begin{bmatrix} C_4 \\ D_4 \end{bmatrix} = [M_3] \cdot \begin{bmatrix} C_3 \\ D_3 \end{bmatrix} \text{ and } \begin{bmatrix} C_5 \\ D_5 \end{bmatrix} = [M_4] \cdot \begin{bmatrix} C_4 \\ D_4 \end{bmatrix} \tag{18}$$

where M_1, M_2, M_3 and M_4 are 2x2 matrices given by:

$$M_1 = \pi \cdot \begin{bmatrix} \left(Ai\left(\xi_I^{-2a}\right) \cdot Bi'\left(\xi_{II}^{-2a}\right) - \frac{K_1}{K_2} Ai'\left(\xi_I^{-2a}\right) \cdot Bi\left(\xi_{II}^{-2a}\right) \right) & \left(Bi\left(\xi_I^{-2a}\right) \cdot Bi'\left(\xi_{II}^{-2a}\right) - \frac{K_1}{K_2} Bi'\left(\xi_I^{-2a}\right) \cdot Bi\left(\xi_{II}^{-2a}\right) \right) \\ \left(\frac{K_1}{K_2} Ai'\left(\xi_I^{-2a}\right) \cdot Ai\left(\xi_{II}^{-2a}\right) - Ai\left(\xi_I^{-2a}\right) \cdot Ai'\left(\xi_{II}^{-2a}\right) \right) & \left(\frac{K_1}{K_2} Ai\left(\xi_{II}^{-2a}\right) \cdot Bi'\left(\xi_I^{-2a}\right) - Bi\left(\xi_I^{-2a}\right) \cdot Ai'\left(\xi_{II}^{-2a}\right) \right) \end{bmatrix} \tag{19}$$

$$M_2 = \pi \cdot \begin{bmatrix} \left(Ai(\xi_{II}^{-a}) \cdot Bi'(\xi_{III}^{-a}) - \frac{K_3}{K_4} Ai'(\xi_{II}^{-a}) \cdot Bi(\xi_{III}^{-a}) \right) & \left(Bi(\xi_{II}^{-a}) \cdot Bi'(\xi_{III}^{-a}) - \frac{K_3}{K_4} Bi'(\xi_{II}^{-a}) \cdot Bi(\xi_{III}^{-a}) \right) \\ \left(\frac{K_3}{K_4} Ai'(\xi_{II}^{-a}) \cdot Ai(\xi_{III}^{-a}) - Ai(\xi_{II}^{-a}) \cdot Ai'(\xi_{III}^{-a}) \right) & \left(\frac{K_3}{K_4} Ai(\xi_{III}^{-a}) \cdot Bi'(\xi_{II}^{-a}) - Ai'(\xi_{III}^{-a}) \cdot Bi(\xi_{II}^{-a}) \right) \end{bmatrix} \quad (20)$$

$$M_3 = \pi \cdot \begin{bmatrix} \left(Ai(\xi_{III}^{a}) \cdot Bi'(\xi_{IV}^{a}) - \frac{K_5}{K_6} Ai'(\xi_{III}^{a}) \cdot Bi(\xi_{IV}^{a}) \right) & \left(Bi(\xi_{III}^{a}) \cdot Bi'(\xi_{IV}^{a}) - \frac{K_5}{K_6} Bi'(\xi_{III}^{a}) \cdot Bi(\xi_{IV}^{a}) \right) \\ \left(\frac{K_5}{K_6} Ai'(\xi_{III}^{a}) \cdot Ai(\xi_{IV}^{a}) - Ai(\xi_{III}^{a}) \cdot Ai'(\xi_{IV}^{a}) \right) & \left(\frac{K_5}{K_6} Ai(\xi_{IV}^{a}) \cdot Bi'(\xi_{III}^{a}) - Ai'(\xi_{IV}^{a}) \cdot Bi(\xi_{III}^{a}) \right) \end{bmatrix} \quad (21)$$

$$M_4 = \pi \cdot \begin{bmatrix} \left(Ai(\xi_{IV}^{2a}) \cdot Bi'(\xi_{V}^{2a}) - \frac{K_7}{K_8} Ai'(\xi_{IV}^{2a}) \cdot Bi(\xi_{V}^{2a}) \right) & \left(Bi(\xi_{IV}^{2a}) \cdot Bi'(\xi_{V}^{2a}) - \frac{K_7}{K_8} Bi'(\xi_{IV}^{2a}) \cdot Bi(\xi_{V}^{2a}) \right) \\ \left(\frac{K_7}{K_8} Ai'(\xi_{IV}^{2a}) \cdot Ai(\xi_{V}^{2a}) - Ai(\xi_{IV}^{2a}) \cdot Ai'(\xi_{V}^{2a}) \right) & \left(\frac{K_7}{K_8} Ai(\xi_{V}^{2a}) \cdot Bi'(\xi_{IV}^{2a}) - Ai'(\xi_{V}^{2a}) \cdot Bi(\xi_{IV}^{2a}) \right) \end{bmatrix} \quad (22)$$

where $\xi_i^{-2a} = \xi_i|_{z=-2a}$ for i=I and II, $\xi_j^{-a} = \xi_j|_{z=-a}$ for j=II and III, $\xi_k^{a} = \xi_k|_{z=a}$ for k=III, IV and $\xi_l^{2a} = \xi_l|_{z=2a}$ for l=IV and V. The parameters K_1 to K_8 are defined as: $K_1 = \xi_I'(z)|_{z=-2a}$, $K_2 = \xi_{II}'(z)|_{z=-2a}$, $K_3 = \xi_{II}'(z)|_{z=-a}$, $K_4 = \xi_{III}'(z)|_{z=-a}$, $K_5 = \xi_{III}'(z)|_{z=a}$, $K_6 = \xi_{IV}'(z)|_{z=a}$ $K_7 = \xi_{IV}'(z)|_{z=2a}$ and $K_8 = \xi_V'(z)|_{z=2a}$.

The eigenvalue equation is obtained by taking C_1=1 and D_1=0 in the following equation and is used to obtain eigenenergies:

$$\begin{bmatrix} C_5 \\ D_5 \end{bmatrix} = [M] \cdot \begin{bmatrix} C_1 \\ D_1 \end{bmatrix}; \text{ where } [M] = [M_4] \cdot [M_3] \cdot [M_2] \cdot [M_1] \quad (23)$$

2.3 Carrier Concentration in the Channel

The electron concentration in the channel at various fields is calculated using the following expression [6]:

$$n(z) = \left(\frac{m^* KT}{\pi \hbar^2} \right) \sum_p \ln \left[1 + \exp \left\{ \frac{(E_f - E_p)}{KT} \right\} \right] \times |\psi_p(z)|^2 \quad (24)$$

where K is the Boltzmann constant, T is the room temperature and E_p is the pth energy level.

III. RESULTS AND DISCUSSION

This work presents a quantum modeling of carrier distribution in symmetric DTQW structure separated by a barrier, formed by two similar heterostructures in a InAlAs-InGaAs-InAlAs DG-HEMT. 1D-Schrodinger equation is solved as described in section-II and numerical calculations using Newton-Raphson technique carried out for calculating eigenvalues and the wavefunctions. The values of material parameters for symmetric double heterostructure $In_{0.52}Al_{0.48}As$/ $In_{0.53}Ga_{0.47}As$ DG-HEMT used in the calculation are as follows: effective mass of $In_{0.53}Ga_{0.47}As$, $m^*=0.033*m_o$ [7], where m_o is the electron rest mass, channel thickness=20 nm, quantum well and barrier thickness = 6.6 nm, V_o=0.5 eV [8] and V_1=0.045 eV.

The symmetric potential profiles of DTQW under equilibrium and at various applied electric fields represented in Fig. 2(b) and Fig. 3 respectively are solved and the eigenvalues thus obtained are presented in Table I. At equilibrium both E_0 and E_1 are less than the Fermi level ($E_F \approx 0.17$ eV) [9] suggesting that mainly these two states are occupied by the electrons and hence are main contributors to the electron concentration in the channel.

TABLE I
EIGENENERGIES WITH DIFFERENT ELECTRIC FIELDS

S.No.	Electric Field 'F'(V/m)	E_0 (eV)	E_1(eV)
1.	0	0.0689	0.1504
2.	$2\text{x}10^6$	0.0683	0.1506
3.	$5\text{x}10^6$	0.0649	0.1518
4.	$7.5\text{x}10^6$	0.0602	0.1532
5.	$10\text{x}10^6$	0.0539	0.1548
6.	$12.5\text{x}10^6$	0.0465	0.1563
7.	$15\text{x}10^6$	0.0380	0.1575

The corresponding wave functions ($\psi_0(z)$) and ($\psi_1(z)$) at equilibrium are shown in Fig. 4. It can be observed that the probability of occupation of the ground state is higher in the barrier region than in the two wells in the absence of any external field. Thus signifying that the electron concentration in the channel has a Gaussian profile and the electrons are no more confined at the two interfaces. Thus, indicating that the DTQW behaves like a single quantum well and the two wells cannot be treated in isolation.

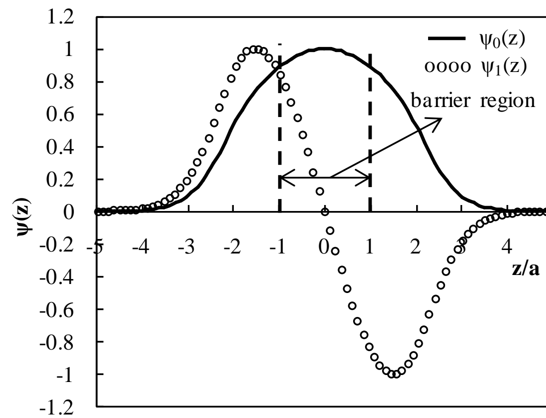

Fig. 4. The ground and first excited DTQW states wave functions at electric field=0.

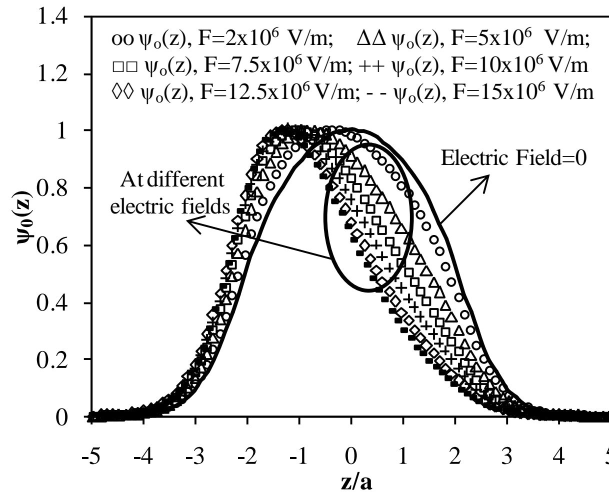

Fig. 5. The behaviour of the ground excited DTQW state wave function, $\psi_0(z)$, under various applied electric fields.

The wavefunctions $\psi_0(z)$ and $\psi_1(z)$ at various transverse electric fields are sketched in Fig. 5 and Fig. 6 respectively. It can be seen from Fig. 5 that as electric field increases, $\psi_0(z)$ keeps on increasing in the well closer to Gate1(held at 0V) and decreases in the well which is closer to Gate2 (at negative potential). So, the probability of occupancy for an electron is shifting towards the interface which is closer to the gate with higher voltage or to the deeper well. The shift in the wavefunction is taking place due to the tunneling in DTQW system. Similarly, Fig. 6 also shows the shift of $\psi_1(z)$ with different applied electric fields. Shifting away of the wavefunction from the interface closer to Gate2 (at negative voltage) indicates that the presence of electric field can initiate a tunneling between the two wells through the barrier region.

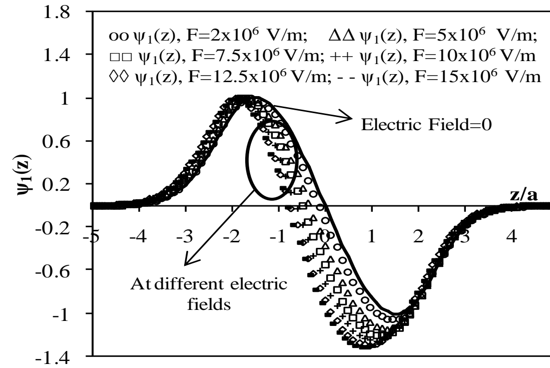

Fig. 6. The behaviour of the first excited DTQW state wave function, $\psi_1(z)$, under various applied electric fields.

Fig. 7 shows a comparison of the electron concentration profile calculated at equilibrium with the simulated results obtained from Quantum moments model and also with a semi- classical model (drift-diffusion model) available in 3D ATLAS Device Simulator. As can be seen from the figure, the analytical electron concentration profile shows a good match with the simulated quantum model and thus validating the proposed model. Also, the peak electron concentration is not at the interface in the quantum model as compared to semi-classical model [10] indicating the merging of the two wells into one.

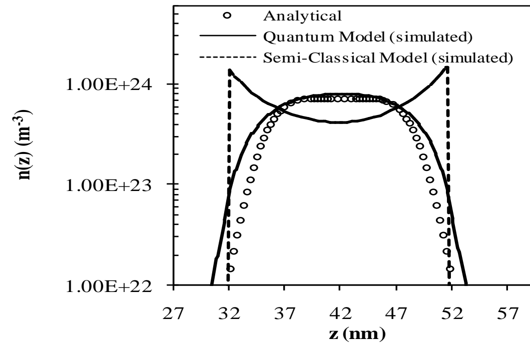

Fig. 7. Comparison of Electron concentration in the channel at equilibrium.

The electron concentration calculated at different applied electric fields is shown in Fig. 8. It is observed that the electron concentration shifts from one side of the channel to the other with applied field. The differential gate voltage, where Gate1 is maintained at 0 V and Gate2 at different operating negative voltages, divided by the channel thickness results in a positive field 'F' in the positive z direction. This positive electric field in the positive z direction pushes the electrons in the negative z direction, and so the potential energy of the electron increases in the positive z direction. This causes shift of electrons away from the interface closer to Gate2 and towards Gate1. The two gates control the electron confinement between the two wells. Shifting of electrons from one interface to the other indicates existence of coupling between the two TQW, which cannot be treated independently and must be solved as a combined system.

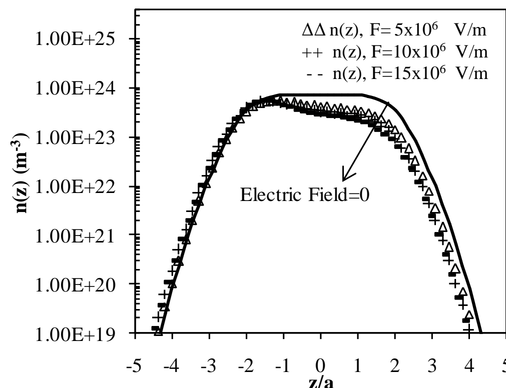

Fig. 8. Electron concentration under various applied electric fields.

IV. CONCLUSION

Nano-dimensional symmetric InAlAs/InGaAs double heterostructure DG-HEMT are promising devices due to their larger carrier concentration and high cut off frequency. The essential results imply that the DTQW in the nanodimensional channel behave like a single triangular quantum well and thus the two wells cannot be treated independently. The eigenvalues obtained from the proposed quantum model at equilibrium are E_0=0.0689 eV and E_1=0.1504 eV. The results show a shift in the wavefunctions from one well to the other depicting an interaction between the two quantum wells. The ground state wavefunction shifts to the deeper well under an applied field or towards the gate which is at a higher gate voltage while it remains symmetric at equilibrium in the two wells. Further, the electron concentration profile in the channel illustrates the distribution and tunneling of electrons under various applied transverse electric fields which establish a correlation or merging of the two quantum wells, making it imperative to account for quantum effects in double heterostructure high speed nano-devices.

Acknowledgements

The authors acknowledge University Grants Commission for providing financial support for this work.

REFERENCES

[1] Y. C. Chen, R. Lai, D. L. Ingram, T. Block, M. Wojtowicz, P. H. Liu, H. C. Yen, A. Oki, D. C. Streit, and K. Yano, "Highly efficient high power InP HEMT amplifiers for high frequency applications," in *Device Research Conf. Dig.*, Denver, USA, pp. 139-140, Jun. 2000.

[2] K. H. G Duh, P. C. Chao, S. M. J Liu, P. Ho, M. Y. Kao and J. M. Ballingall, "A super low-noise 0.1 um T-Gate InAlAs-InGaAs-InP HEMT," *IEEE Microw. Guided Wave Lett., vol. 1(5),* 1991, pp. 114-116,

[3] N. Wichmann, I. Duszynski, S. Bollaert, J. Mateos, X. Wallart, and A. Cappy, "100 nm InAlAs/InGaAs double-gate HEMT using transferred substrate," in *IEDM Tech. Dig.*, 2004, pp. 1023–1026.

[4] M. Bhattacharya, J. Jogi, R. S. Gupta, and M. Gupta, "Impact of Doping concentration and Donor-layer thickness on the dc characterization of symmetric Double-gate and Single-gate InAlAs/InGaAs/InP HEMT for nanometer gate dimension-A comparison," in IEEE TENCON, 2010, pp. 134- 139.

[5] ATLAS User's Manual (version: 5.16.3.R), Silvaco International; 2010.

[6] A. P. Gnädinger, and H.E. Talley, "Quantum mechanical calculation of the carrier distribution and the thickness of the inversion layer of a MOS Field-Effect Transistor," *Solid-State Electronics, vol. 13(9),* 1970, pp. 1301-1309.

[7] J. B. Restorff, B. Houston, J. R. Burke, and R.E. Hayes, "Measurement of effective mass in In0.9Ga0.1As0.22P0.78 by Shubnikov–de Haas oscillations," *Appl. Phys. Lett., vol. 32(3),* 1978, pp. 189-190.

[8] Y. Kwon, D. Pavlidis, M. Tutt, G. I. Ng, and T. Brock, "W-band Monolithic Mixer using InAlAs/InGaAs HEMT," in *IEEE GaAs IC Symp. Tech. Dig.,* LA, USA, 1990, pp. 181-184.

[9] N. Dasgupta, and A. Dasgupta, "An analytical expression for sheet carrier concentration versus gate voltage for HEMT modeling," *Solid State Electronics, vol. 36(2),*1993, pp. 201-203.

[10] N. Verma, M. Gupta, R.S. Gupta, and J. Jogi, "Quantum Modeling of Nanoscale Symmetric Double-Gate InAlAs/InGaAs/InP HEMT", *JSTS Journal of Semiconductor Technology and Science, vol. 13(4),* 2013, pp. 342-354.